Sheet plasmons in modulated graphene on Ir(111)

2011 New J. Phys. 13 053006

(http://iopscience.iop.org/1367-2630/13/5/053006)

New Journal of Physics
The open-access journal for physics

Sheet plasmons in modulated graphene on Ir(111)

T Langer[1,2], D F Förster[3], C Busse[3], T Michely[3], H Pfnür[1] and C Tegenkamp[1,4]

[1] Institut für Festkörperphysik, Leibniz Universität Hannover, Appelstrasse 2, D-30167 Hannover, Germany
[2] Physikalisch-Technische Bundesanstalt, Bundesallee 100, D-38116 Braunschweig, Germany
[3] II Physikalische Institut, Zülpicher Street 77, D-50937 Köln, Germany
E-mail: tegenkamp@fkp.uni-hannover.de

New Journal of Physics **13** (2011) 053006 (12pp)
Received 20 January 2011
Published 3 May 2011
Online at http://www.njp.org/
doi:10.1088/1367-2630/13/5/053006

Abstract. The sheet plasmon of graphene on Ir(111) was investigated in this paper by means of high-resolution electron energy loss spectroscopy. The perfect lateral coordination of sp^2-hybridized C atoms on a large scale is manifested by brilliant moiré diffraction images. However, the modulation of the graphene films caused by hybridization at the interface limits the lifetimes of the collective excitation modes. This modulation within the films can be lowered owing to intercalation of Na. Linear dispersion was found, but surprisingly the overall slope of the dispersion is not dependent on the chemical potential within the graphene films. The dispersion measured for graphene on Ir(111) is almost identical to that measured on SiC(0001), although the carrier densities differ by two orders of magnitude. This contradicts the model that the relevant carrier density for a two-dimensional plasmon is given by $(2\pi)^{-1}k_F^2$.

[4] Author to whom any correspondence should be addressed.

Contents

1. Introduction

Graphene, with its peculiar band structure, is a two-dimensional (2D) electron gas with outstanding electrical properties [1, 2]. The continual optimization of processing parameters now allows the growth of perfectly coordinated sp^2-hybridized C atoms crystallized in a honeycomb lattice on the micrometer scale [3]–[5]. The combination of these methods with nanostructuring opens up new pathways to graphene-based device structures [6].

Single graphene layers can be obtained by exfoliation of graphite, by sublimation of Si on SiC surfaces or by decomposition of hydrocarbons on transition metal surfaces [7]–[10]. The system under investigation here, namely graphene grown epitaxially on Ir(111), is distinct from other systems, as the graphene layer contains a very low number of defects and single domains extend over micrometers [11]. Furthermore, due to the chemical inertness of graphene itself and the low solubility of carbon in the Ir bulk, the growth process is self-limiting and always leads to one, and only one, layer of graphene [12]. The chemical interaction between the Ir substrate and graphene is rather weak, as evidenced by a nearly unperturbed band structure [13, 14] and a long vertical distance between the C and Ir atoms [20], in contrast to other systems such as graphene/Ni(111) or graphene/Ru(0001), where the strong hybridization of electronic bands opens up a gap in the Dirac cone. In addition, graphene on Ir(111) is nearly undoped, whereas for example graphene on SiC(0001) shows strong n-doping as a result of charge transfer between graphene and the substrate. As a consequence of the weak interaction, graphene on Ir(111) overgrows substrate steps in a carpet-like mode [12]. On metal surfaces with significant lattice mismatch with respect to graphene, moiré superstructures appear [15]–[17] and, more noticeably, the films reveal corrugations which correlate with the strength of the chemical bonding at the interface [18, 19]. Even in the case of weakly interacting graphene on Ir(111) in special regions of the moiré, a significant overlap of the electronic systems of the metal and the carbon lattice occurs [20].

The spectroscopy of low-dimensional plasmons in graphene reveals important and supplementary information through the electronic response of the electrons close to the Fermi level. Referring to the approximation of a nearly free 2D electron gas (NFEG), the plasmon energy depends on the electron effective mass and the density of states at Fermi energy [21]. For graphene with linearly dispersing bands, a $\sqrt{k}$ behavior of the plasmon energy as a function of the scattering vector is still expected [22]. Several attempts have been made recently to calculate accurately the plasmon dispersion including inter- and intra-band

transitions, intra- and inter-valley scattering and static and dynamic screening effects [22, 23]. However, structural imperfections [24], finite lifetimes of plasmons, resonance effects with single particle excitations [25] and their feedback to the collective plasmon have not been considered theoretically so far.

Recent electron energy loss investigations have shown that graphene is indeed an ideal template for studying the influence of the above-mentioned parameters. In particular, the spatial extension of this quasiparticle can be exploited to probe the influence of surface roughness. By systematic variation of the graphene terrace widths it was shown that the lifetime of the 2D plasmons is proportional to the terrace size [24]. Furthermore, using electron-doped graphene ($E_F \approx 500$ meV) the importance of interband transitions and the feedback to the plasmon frequency have been demonstrated [25]. The plasmon electron–hole coupling causes a redshift in the dispersion and its position depends on the chemical potential as supported by adsorption experiments with F4-TCNQ, while the average slope of the dispersion remains unchanged.

From this point of view, graphene grown on Ir(111) is the interesting counterpart: the intrinsic defect concentration is significantly lower [15] and the film is almost undoped [13]; that is, only plasmon dispersion can be measured and intrinsic interband transitions as for graphene on SiC(0001) are not expected. In particular, the ultra-low carrier densities in these films should have an effect on the slope of the dispersion ($\omega_p \propto N^{1/4}$ [22]). Most surprisingly, as we show in this paper, the dispersion is rather insensitive to the chemical potential. This effect can be qualitatively explained by considering the finite lifetimes of the plasmons. Furthermore, despite the low step and point defect concentrations within these films, the full-width at half-maximum (FWHM) of the main loss structure is significantly higher than that for graphene on SiC(0001) [25]. Compared to graphene on SiC substrates grown by sublimation, these films hardly contain defect structures of atomic size such as steps or grain boundaries, except the buckling of the film on terraces and at step sites. As it turns out, the modulation of graphene on the terraces itself is responsible for the strong damping of the plasmons.

2. Experimental setup

The measurements were carried out under ultra-high vacuum (UHV) conditions (5×10^{-8} Pa). The chamber was equipped with a high-resolution electron loss spectrometer (EELS) used as the electron source and detector of a low-energy electron diffraction system (LEED) that allows simultaneous high momentum ($k_\parallel$) resolution [26]. Typical operating parameters were 25 meV energy resolution at a $k_\parallel$ resolution of 1.3×10^{-2} Å^{-1} in the energy range between 15 and 70 eV [26]. In order to image full Brillouin zones and use higher electron energies, the vacuum system also hosted a high-resolution spot profile analysis (SPA)–LEED system.

Ordered and clean Ir(111) surfaces were generated by repeated cycles of Kr^+-sputtering between 300 and 1100 K, followed by subsequent flash annealing to 1530 K. For graphene growth ethylene was adsorbed at room temperature until the sample surface was saturated, followed by thermal decomposition of the hydrocarbon at 1500 K, resulting in a fraction of 0.22 of the Ir(111) surface being covered by graphene flakes. The graphene sheet was then completed by exposing the sample to 1×10^{-5} Pa of ethylene for 1200 s at 1200 K. This two-step process yields nearly defect-free extended monolayer graphene sheets with the $\langle 11\bar{2}0 \rangle_C$-direction aligned to the $\langle 1\bar{1}0 \rangle_{Ir}$-direction [11]. The samples were grown in a different UHV system and transferred afterwards into the EELS–LEED system. Mild annealing to 700 K for several minutes leads to full desorption of water and other contaminants, and SPA–LEED

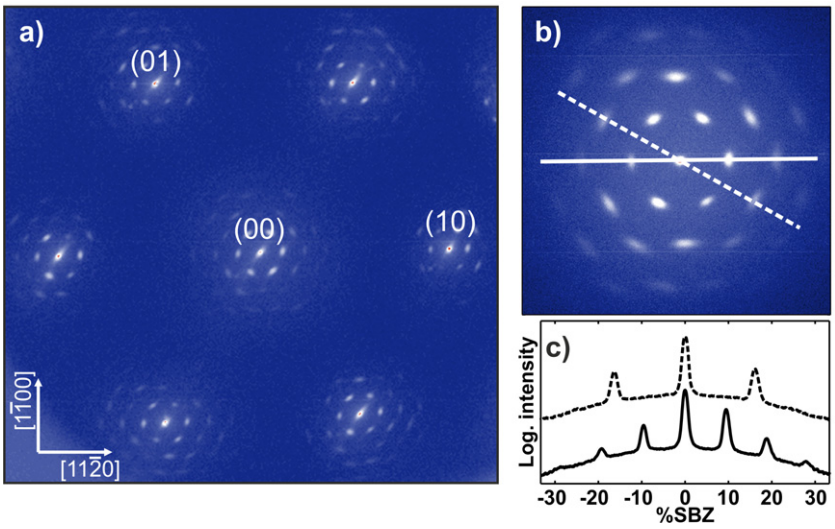

Figure 1. (a) SPA–LEED pattern of graphene on Ir(111) showing the first surface Brillouin zone (SBZ). Electron energy 233 eV. (b) Magnification of the central (00)-spot taken at 153 eV. (c) Line scans taken along the directions indicated in panel (b). Measurements were made at room temperature.

reveals a brilliant diffraction pattern of a graphene monolayer structure. Sodium was used for adsorption and deposited from an outgassed dispenser (SAES getters), keeping the pressure in the 10^{-7} Pa regime.

3. Results and discussion

3.1. Structure

The extremely high quality of graphene on Ir(111) surfaces is demonstrated by the LEED pattern shown in figure 1. After the transfer of the sample into UHV and annealing to 500 K, the diffraction patterns reveal the full moiré structure between the substrate and the graphene lattice. Up to fourth-order moiré diffraction spots are visible, representing an extremely long-range ordered film with ultra-low defect densities, as demonstrated by figure 1(b) and corresponding line scans (figure 1(c)). The SBZ has been calibrated with respect to the graphene lattice; that is, the first-order moiré spots appear around 9.5% SBZ [14].

The FWHM of the central peak measured at 153 eV (scattering phase $S = 4.5$, step height $d = 2.21$ Å) is around 1% SBZ and is essentially governed by the mosaicity of the Ir crystal (0.2° as determined using x-ray diffraction). Consequently, the average terrace size cannot be determined directly from the width of this peak. However, STM results show that the average terrace sizes are as large as 50 nm [15]. The FWHM of the moiré spots along the radial directions does not depend on the spot order. In contrast, the FWHM along the polar direction is increasing, as shown by figure 2. Although the FWHM of six equivalent spots varies, the broadening is clearly visible. From the slope of the least-quare fit (solid line in figure 2(c)) a rotational disorder of ±4.2° of the moiré superstructure is deduced. The moiré pattern amplifies the rotational misalignment of the graphene lattice with respect to the underlying Ir lattice by a factor of 10.6 [15]; therefore the rotational disorder of the graphene is ±0.39°, which agrees

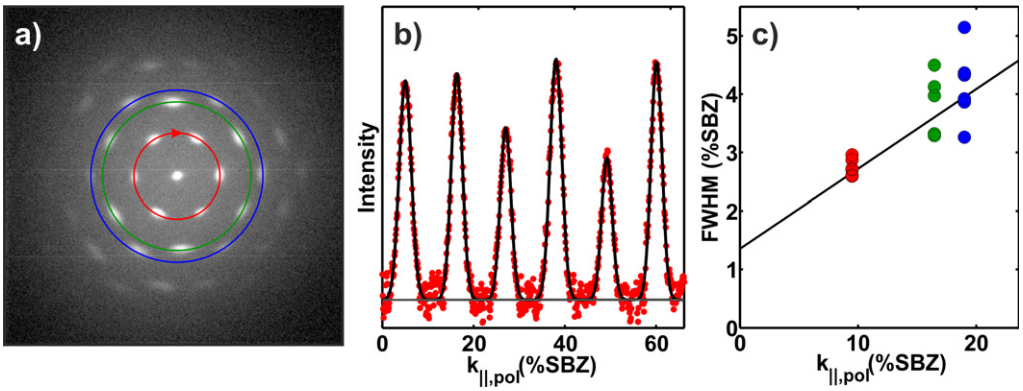

Figure 2. (a) 2D LEED pattern of the moiré spots. Along the circles line scans were taken, as shown exemplarily for the inner spots in (b). (c) With higher diffraction order, the FWHM increases, which indicates rotational disorder of the graphene films. The polar direction has been re-calibrated in %SBZ. The electron energy of 153 eV corresponds to a scattering phase $S = 4.5$, assuming a step height of 2.21 Å.

reasonably with STM measurements [15]. Other rotational domains, as reported in [16], are not present.

3.2. Sheet plasmon

The loss spectra for monolayer graphene grown on Ir(111) have been measured in detail for scattering vectors ranging from zero to 0.14 Å^{-1}. As we will show below, the dispersing loss peak is related to the sheet plasmon of graphene. However, before the details of the dispersion itself are presented, some general remarks on the loss spectrum of graphene on highly polarizable Ir(111) surfaces will be made. In particular, a comparison with the graphene sheet plasmon on SiC(0001) reveals new insights into the nature of this collective excitation mode: figure 3(a) shows the loss spectrum of graphene/Ir(111) exemplarily taken at a finite scattering vector ($k = 0.057$ Å^{-1}), at which the plasmon loss is clearly separated from the elastic peak. The most intense loss feature around $\hbar\omega_p \approx 500$ meV can be assigned to the sheet plasmon. Compared to the plasmon of graphene on SiC(0001) (figure 3(b)), which has recently been investigated [24, 25], the graphene sheet plasmon on Ir(111) is less intense by a factor of five, while the FWHM is twice as large. As the intensity of losses measured by EELS is related to charge fluctuations at the surface, a comparatively low intensity is expected for graphene films with a very low charge carrier density near E_F. The spectra were measured at room temperature and the primary energy was 20 eV. The FWHMs of the elastic peaks were around 25 meV and are not responsible for the FWHM of the loss structure. At first glance this finding is unexpected since the quality of catalytically grown graphene films is apparently better, because the in-plane coordination of the C atoms is perfect, compared to those grown by sublimation. Also, the global interaction of graphene with Ir(111) is weaker than for SiC(0001), as evidenced by the small graphene band measured using angle-resolved photoemission spectroscopy (ARPES) [7, 13, 14].

We have recently shown that steps or grain boundaries within the graphene film effectively limit the lifetime of plasmons in a way in which phase space arguments play only a minor

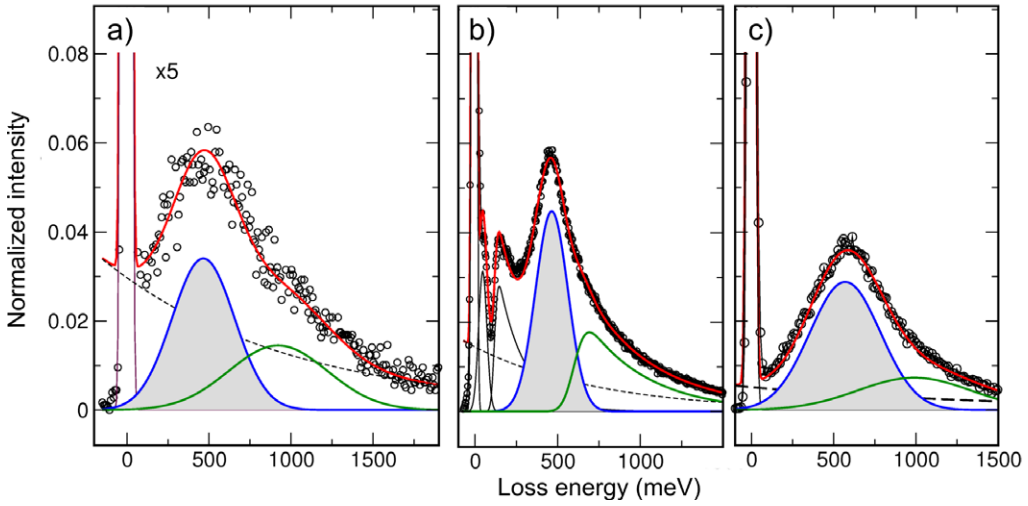

Figure 3. EEL spectra of graphene on (a) Ir(111), (b) SiC(0001) and (c) Ir(111) with Na taken at $k = 0.057\,\text{Å}^{-1}$. The average terrace widths are 50, 150 and 50 nm, respectively. The relevant contributions, i.e. phonons (thin solid lines, only visible on SiC (b)), the Drude background (dashed lines) and the sheet plasmon (blue and green thick solid lines) are marked. The electron energy was 20 eV. All EEL spectra shown throughout the paper are normalized with respect to the elastic peak. For further details, see text.

role [24]. Since the phase velocities of plasmons and electrons are almost identical, only momentum transfer is necessary for conversion of plasmons into electron–hole pairs and imperfections such as steps act as arbitrary momentum sources. Thus, intra-band transitions are energetically possible and compete with the collective excitations. The FWHM of the plasmons measured for graphene/Ir(111) (figure 3(a)) is almost the same as that of graphene/SiC(0001) with an average terrace length of 20 nm. However, the step density is significantly lower in this case. Therefore, the strong damping cannot solely be explained by strongly bent graphene at step edges. Since the rotational disorder is rather small and the individual domains extend over 100 nm, this defect structure is also of minor relevance for the lifetime of the sheet plasmons. This means that the modulation of graphene itself must be responsible for the damping of the plasmons. Although, in contrast to uncorrelated step structures, the modulation can provide only a well-defined momentum, the transfer of plasmons into the Landau regime still seems to be an effective mechanism. The experiments with intercalated Na support this model (see below). Due to the intercalation of Na the modulation of the graphene film is reduced and, accordingly, the lifetimes of the plasmons increase in the regime of short plasmon wavelengths. This modulation is coupled with the degree of hybridization at the interface [20], which may provide the necessary channel for damping on the local scale. Thus the coupling of the electronic systems of graphene with the electron gas of the metal can open up an effective decay channel for sheet plasmons. Such an enhanced electronic coupling feeds back even to lattice vibrations. For graphene orientations like in our case, the characteristic G- and 2D-modes were not found in Raman spectroscopy [19].

Furthermore, as is obvious from figure 3, the plasmon spectra reveal a second loss structure that is located at $2\hbar\omega_p$. It was claimed recently that this loss structure is also present for graphene

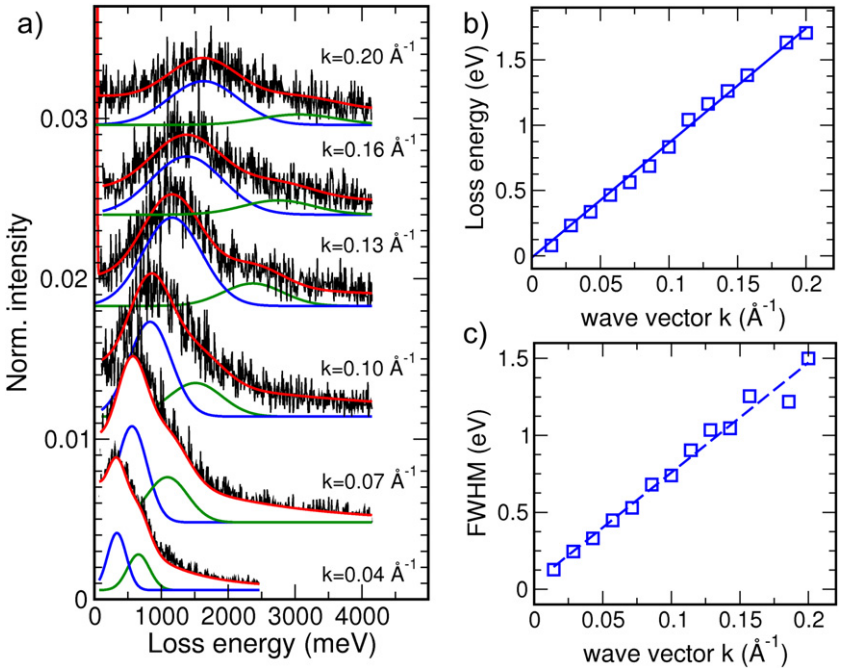

Figure 4. (a) Energy loss spectra for graphene on Ir(111) at different scattering wave vectors. Two loss peaks are clearly visible and these are assigned to the ordinary sheet plasmon (blue □) and a multipole mode (green line). For better visibility spectra are shifted. More details of the fitting are explained in the context of figure 3. Panels (b) and (c) show the dispersion and FWHM of the ordinary sheet plasmon, respectively.

grown on SiC(0001). However, in the present case the relative intensity compared to the main loss feature is significantly higher than on SiC. While the ratio between the sheet plasmon and this high energy mode is 3 : 1 on SiC, on Ir(111) it is close to 3 : 2. After adsorption of Na, the intensity of the sheet plasmon increases, the FWHM is reduced and in particular the ratio between the two losses is again 3 : 1. Thus details of the charge distribution at the interface seem to be important for this mode. In analogy to surface plasmons located at two interfaces and interacting with each other [29, 30], the $2\hbar\omega_p$ mode can be assigned to a multipole plasmon mode. Details will be discussed elsewhere [31].

According to the fit models shown in figure 3 the loss spectra have been analyzed for different scattering vectors. Exemplarily, some spectra are shown in figure 4(a), together with the loss energies and FWHMs deduced from the analysis. These are plotted versus the scattering vector parallel to the surface in figures 4(b) and (c). Since the cross section for scattering increases with decreasing plasmon wavelength, the FWHM is linearly increasing in agreement with previous investigations [24]. The gradual increase of FWHM in the whole wave vector regime further implies that an additional damping mechanism for plasmons with a wavelength smaller than the average terrace width of the substrate must be present, and supports the conclusion mentioned above that the modulation itself is decisive.

Despite the significant broadening of the plasmon modes in this system, it is still possible to measure the dispersion with high accuracy, particularly in the range of low scattering vectors,

because the phonon modes on Ir(111) are significantly lower in energy than on SiC(0001). The high-energy Fuchs–Kliewer mode on SiC is around 150 meV (cf figure 3(b)). The dispersion of the sheet plasmon (squares) is shown in figure 4(b) and reveals several interesting findings.

Firstly, the dispersion of the 2D plasmon is almost identical to that measured on SiC(0001) [25, 27], although the carrier concentrations differ by two orders of magnitude. This finding is in clear contrast to NFEG systems, e.g. Si(111)—Ag$\sqrt{3}$ [28], where the effect of doping has been seen by a shift in the plasmon energy. For graphene the average slopes on Ir(111) and SiC(0001) are 8.2 ± 0.5 eV Å and 8.4 ± 0.4 eV Å, respectively. According to plasmon theory [21], the slope is determined by the electron density (for graphene $\omega_p \propto N^{1/4}$ [22]), the effective mass and the dielectric constant of the substrate. Assuming hypothetically identical carrier concentrations in both graphene systems, the higher dielectric constant of Ir should already lead to a pronounced redshift of the dispersion as a whole. Obviously, this is not the dominant factor.

In order to explain the similarity of the dispersion slopes, either the *N/m* ratio is constant or the *effective* electron density N_{eff} differs from the carrier density calculated via $2\pi N = k_F^2$ for 2D systems. In NFEG systems, where the conduction band is separated by a band gap from the valence states, the plasmon frequency is indeed proportional to k_F [28]. However, as it turns out, the equivalence of N_{eff} and the carrier density within the conduction band are different if half-metallic systems are considered. Our results reveal that for graphene the dispersion is to first order not dependent on k_F. Instead, the effective charge carrier density is given by an integration over a certain width in energy space which is k-value independent. Although the origin of this window remains unclear at the moment, the k-dependence of the FWHM of the plasmons (cf figure 4(c)) itself is only of minor relevance to the slope of the dispersion, because otherwise the slope would be affected by the defect concentration, which is in contrast to recent EELS experiments [24, 25].

Secondly, the plasmon dispersion is rather linear (figure 4(b)). Of course, ultra-low effective masses also give rise to a linear dispersion. For graphene on SiC(0001), where an effective mass of $0.06m_e$ was assumed, clear deviations from this linearity have been seen for long wavelengths [25]. Thus, the effective mass for graphene on Ir(111) should be as low as $0.000\,6m_e$ in order to compensate for the different charge carrier densities in both systems. However, this contradicts the conclusion that the modulation of graphene films, and hence the coupling to the Ir surface, feeds back to the lifetimes of the plasmons. A further argument, which could explain the linearity, is adopted from recent HREELS measurements where the collective mode of the 2D surface states on Be(0001) [32] and Cu(111) [33] has been investigated. Due to screening, the low-dimensional plasmons show an acoustic, i.e. linear, behavior. Whereas on Be(0001) the collective mode of the surface states is screened by bulk bands, in our case the graphene is screened by Ir states. These considerations, although they can only explain our data qualitatively, show that the band structure and, in addition, structural parameters need to be considered.

3.3. Na adsorption

As seen, the delicate interplay between physisorption and hybridization at the interface causes a corrugation of the graphene sheet [18, 20]. To modify the interaction strength and/or the chemical potential, adsorption experiments with Na were performed.

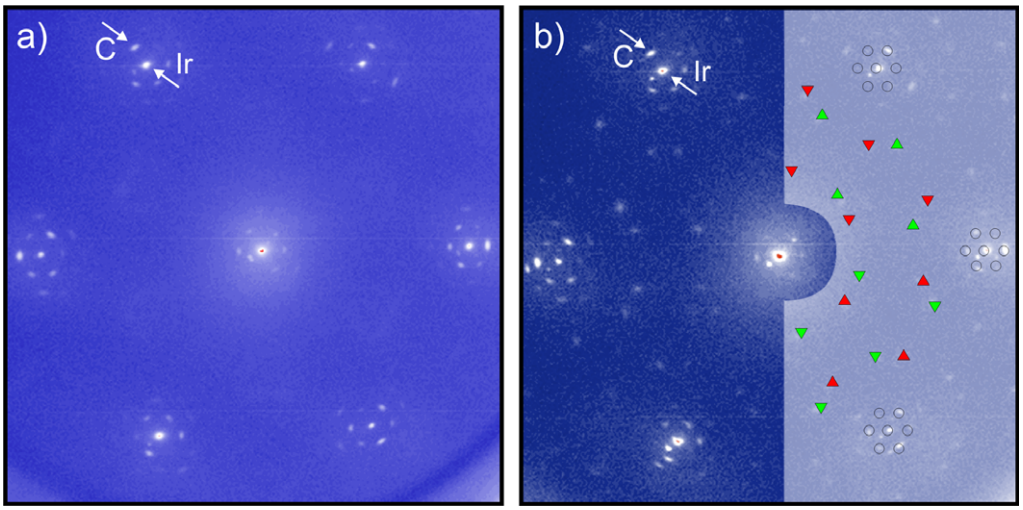

Figure 5. LEED pattern showing the first Brillouin zone of graphene/Ir(111) after the adsorption of Na at room temperature. With increasing amount of Na, the high-order moiré peaks vanish gradually and new reconstruction spots appear: (a) diffuse intensity at $\sqrt{3} \times \sqrt{3}$ positions after 1 min; (b) after 2 min of Na adsorption, $\sqrt{7} \times \sqrt{7}$ mirror domain structures appear. A schematic diagram of the moiré structure (circles) and the domains (triangle up, triangle down) is shown in the right half of panel (b). The electron energy was 230 eV.

Before the loss spectra are presented, a closer look at the structure after adsorption of Na is necessary. The LEED patterns shown in figure 5 were obtained after 1 and 2 min of Na adsorption, respectively. The vanishing of the high-order moiré diffraction spots shows that the interaction between graphene and Ir is significantly reduced by Na adsorption, resulting in a reduced modulation amplitude. Whereas after 1 min very faint indications of a $\sqrt{3} \times \sqrt{3}$ reconstruction become visible, after 2 min of adsorption $\sqrt{7} \times \sqrt{7}$ reconstructions are obvious. In this particular case the analysis of the LEED structure has revealed a mirror domain structure, as sketched in figure 5(b). Although the absolute coverage has not been calibrated, the reconstructions suggest that at least 0.3–0.7 ML have been deposited. Most important, the reconstruction spots appear with respect to the Ir(111) surface, a strong indication that Na intercalates.

A sequence of EEL spectra taken at the structure shown in figure 5(b) is plotted in figure 6(a). Although Na-induced reconstructions are visible, the 2D plasmon is still present. The data were fitted with the model presented in the context of figure 3. The dependence of the FWHM as a function of the scattering vector is shown in figure 6(c). Whereas up to $k_c = 0.11\,\text{Å}^{-1}$ the FWHMs are identical to those measured for pristine graphene, they differ clearly for high k-values. The decrease of FWHM is unexpected since adsorbates should further lead to a supplementary damping of plasmons, as seen in the case of Na adsorption on graphene on SiC(0001) [37].

Relying on the damping model presented above and in agreement with the LEED findings, the reduction of the FWHM for the plasmons is a clear indication that the coupling of the graphene film to the substrate is reduced to some extent. A change in the structure upon intercalation is plausible as the modulation originates from charge redistribution at the

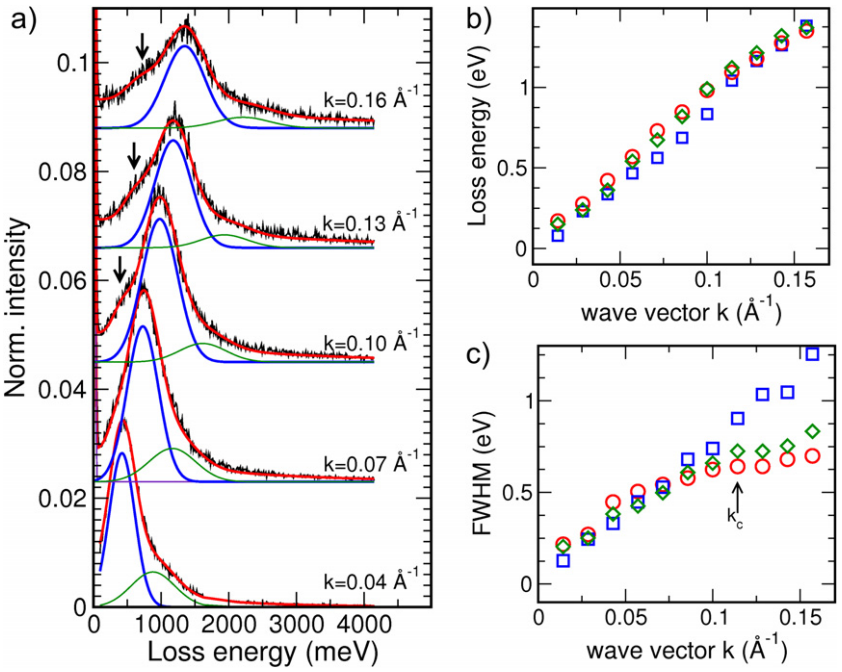

Figure 6. (a) EEL spectra of graphene/Ir(111) after adsorption of Na for 1 min. Only the two characteristic plasmon modes are marked (thick (blue) and thin (green) solid lines.) (b) Dispersion of clean graphene and that measured after adsorption of Na (1 min, red ○; 2 min, green ◇). For comparison, the data of dispersion for clean graphene is also shown (blue □). (c) FWHM of the sheet plasmon. The symbols (colors) are the same as in panel (b).

interface [18]. The fundamental plasmon mode, at which a saturation of FWHM is seen in figure 6(c) (characterized by $\lambda/2 = 2\pi/k_c$), correlates reasonably with the moiré superstructure of 2.5 nm. In contrast, the FWHM behavior in the long wavelength regime remains unchanged; that is, Na-induced step redistribution on the Ir(111) surface does not occur.

The corresponding dispersion is shown in figure 6(b). The dispersion after adsorption is almost identical to the dispersion of pristine graphene (squares). Only at low k-values the loss energies are slightly higher (15%). In general, the adsorption of metal atoms leads to a significant shift of the chemical potential. Depending on the work function, both p- and n-type doping can be achieved [36]. The intercalation of electropositive Na should cause a pronounced shift of the Fermi energy above the neutrality point. Assuming a moderate charge transfer of 0.1 electron per Na atom, the carrier concentration is of the order of 1×10^{14} cm^{-2}. Adsorption of Eu has shifted the Fermi energy by more than 1 eV above the Dirac point, resulting in a similar carrier concentration [35]. However, the dispersion of graphene is rather insensitive to such doping experiments. This supports our conclusion that not all (and not only) electrons in the conduction band are participating in the plasmon state.

As mentioned, and as is obvious from a close inspection of figure 6(b), the dispersion around 800 meV of clean graphene deviates slightly from the one measured after adsorption of Na. This small shift of the dispersion to higher loss energies seen at low k-values is much smaller than that expected from theory [22]; therefore, other scenarios may also contribute. We have recently shown, for graphene on SiC(0001), that the coupling of the plasmons to other

quasiparticles can lead to redshifts in the dispersion [25]. The position of the dip coincides with the chemical potential of the conduction band and was explained by resonant excitation of electron–hole pairs within graphene [25]. For graphene on Ir(111), where the Dirac point is very close to the Fermi level [13, 14], such an intrinsic damping mechanism is not expected. Nonetheless, the proposed resonance model described in [25] is not necessarily restricted to intrinsic interband decay channels. Interband transitions can also take place between states located at graphene and interface sites. Indeed, the clean Ir(111) surface has occupied surface states located at around 800 meV below E_F at the $\bar{\Gamma}$ point [34]. While the Ir surface states are still visible in spectroscopy with graphene atop [13], they vanish or, at least, are changed by intercalated Na. The moiré structure seen in LEED is reflected by strong replica band structures in ARPES [13]. However, their energetic positions in k-space are not in resonance with the plasmon dispersion. Thus a strong influence of the moiré structure on dispersion is not expected. Furthermore, a close inspection of the loss spectra shown in figure 6(a) reveals a shoulder at lower loss energies (see arrows). The shift is stronger than expected for optical phonons; thus the shoulder may be related to a sheet plasmon originating from the Na reconstruction at the interface. In principle, both sheet plasmons may interact with each other; thus the energy of the graphene plasmon is shifted to higher loss energies [30]. However, this is speculative at this point and more systematic adsorption experiments are needed in order to elucidate further this interesting scenario of interacting plasmons.

4. Summary and conclusion

In summary, we have analyzed the dispersion of undoped and modulated graphene films grown on Ir(111) using angle-resolved electron energy loss spectroscopy. The modulation of graphene on the terraces by moiré formation is a source of effective plasmon damping, which can be lifted to some extent by adsorption of Na, which intercalates almost fully even though adsorption was performed at room temperature. Most surprisingly, the slope of the dispersion is rather insensitive to the chemical potential, as revealed by adsorption of Na and by comparison with pristine graphene grown on SiC(0001). Although the interplay between the effective mass, effective carrier density and screening effects remains unclear at this point, our study has clearly revealed that the relevant plasmon carrier concentration differs from the carrier density within the conduction band. Both findings clearly show that half-metallicity as well as structural disorder and periodic modulations are key parameters in order to describe plasmons of graphene reliably.

Acknowledgments

We acknowledge financial support from DFG.

References

[1] Novoselov K S, Geim A K, Morozov S V, Jiang D, Zhang Y, Dubonos S V, Grigorieva I V and Firsov A A 2004 *Science* **306** 666

[2] Tzalenchuk A, Lara-Avila S, Kalaboukhov A, Paolillo S, Syväjärvi M, Yakimova R, Kazakova O, Janssen T J B M, Fal'ko V and Kubatkin S 2009 *Nat. Nanotechnol.* **5** 186

[3] Emtsev K V *et al* 2009 *Nat. Mat.* **8** 203

[4] Virojanadara C, Syväjärvi M, Yakimova R and Johannson L I 2008 *Phys. Rev.* B **78** 245403
[5] Virojanadara C, Yakimova R, Osiecki J R, Syväjärvi M, Uhrberg R I G, Johansson L I and Zakharov A A 2008 *Surf. Sci.* **603** L87
[6] Sprinkle M, Ruan M, Hu Y, Hankinson J, Rubio-Roy M, Zhang B, Wu X, Berger C and de Heer W A 2010 *Nat. Nanotechnol.* **5** 727
[7] Ohta T, Bostwick A, Seyller Th, Horn K and Rotenberg E 2006 *Science* **313** 951
[8] Geim A K and Novoselov K S 2007 *Nat. Mater.* **6** 183
[9] Coraux J, N'Diaye A T, Busse C and Michely T 2008 *Nano Lett.* **8** 565
[10] Sutter P W, Flege J I and Sutter E A 2008 *Nat. Mater.* **7** 406
[11] Van Gastel R, N'Diaye A T, Wall d, Coraux J, Busse C, Buckanie N M, Meyer zu Heringdorf F-J, Horn-von Hoegen M, Michely T and Poelsema B 2009 *Appl. Phys. Lett.* **95** 121901
[12] Coraux J, N'Diaye A T, Busse C and Michely T 2008 *Nano Lett.* **8** 565
[13] Pletikosić I, Kralj M, Pervan P, Brako R, Coraux J, N'Diaye A T, Busse C and Michely T 2009 *Phys. Rev. Lett* **102** 056808
[14] Rusponi S, Papagno M, Moras P, Vlaic S, Etzkorn M, Sheverdyaeva P M, Pacilé D, Brune H and Carbone C 2010 *Phys. Rev. Lett.* **105** 246803
[15] N'Diaye A T, Coraux J, Plasa T N, Busse C and Michely T 2008 *New J. Phys.* **10** 043033
[16] Loginova E, Nie S, Thürmer K, Bartelt N C and McCarty K F 2009 *Phys Rev.* B **80** 085430
[17] Wintterlin J and Bocquet M L 2009 *Surf. Sci.* **603** 184
[18] Preobrajenski A B, Ling Ng M, Vinogradov A S and Mårtensson N 2008 *Phys. Rev.* B **78** 073401
[19] Starodub E, Bostwick A, Moreschini L, Nie S, El Gabaly F, McCarty K F and Rotenberg E 2010 arXiv:1012.2826v1
[20] Busse C *et al* submitted
[21] Stern F 1967 *Phys. Rev. Lett.* **18** 546
[22] Hwang E H and Das Sarma S 2007 *Phys. Rev.* B **75** 205418
[23] Hill A, Mikhailov A and Ziegler K 2009 *Eur. Phys. Lett.* **87** 27005
[24] Langer T, Baringhaus J, Pfnür H, Schumacher H W and Tegenkamp C 2010 *New J. Phys.* **12** 033017
[25] Tegenkamp C, Pfnür H, Langer T, Baringhaus J and Schumacher H W 2011 *J. Phys.: Condens. Matter* **23** 012001
[26] Claus H, Büssenschütt A and Henzler M 1992 *Rev. Sci. Instrum.* **4** 2195
[27] Liu Y, Willis R F, Emstev K V and Seyller Th 2008 *Phys. Rev.* B **78** 201403
[28] Nagao T, Hildebrandt T, Henzler M and Hasegawa S 2001 *Phys. Rev. Lett.* **86** 5747
[29] Quinn J F 1992 *Solid State Commun.* **84** 139
[30] Liebsch A 1997 *Electronic Excitations a Metal Surfaces* (New York: Plenum)
[31] Pfnür H, Langer T, Baringhaus J and Tegenkamp C 2011 *J. Phys.: Condens. Matter* **23** 112204
[32] Diaconescu B *et al* 2007 *Nature* **448** 57
[33] Pohl K, Diaconescu B, Vercelli G, Vattuone L, Silkin V M, Pitarke J M, Chulkov E V, Echenique P M and Rocca M 2010 *Eur. Phys. Lett.* **90** 57006
[34] Pletikosić I, Kralj M, Šokčevi'c D, Brako R, Lazić P and Pervan P 2010 *J. Phys.: Condens. Matter* **22** 135006
[35] Förster D F, Busse C and Michely T unpublished work
[36] Giovannetti G, Khomyakov P A, Brocks G, Karpan V M, van den Brink J and Kelly P J 2008 *Phys. Rev. Lett.* **101** 026803
[37] Langer T *et al* Adsorption of Na on graphene/SiC(0001) lead to a broadening of the FWHM of the plasmons (unpublished work)